Faraday Discussions
Cite this: *Faraday Discuss.*, 2026, **263**, 426



PAPER





# Hot-drawing ionic liquid-spun lignin–poly(vinyl alcohol) fibres increases strength and polymer alignment

Enny Tran, †[ab] Joanne Pui Fai Ng, †[b] Lucie Diéval,†[c] Stéphan Rouzière,[c] Pascale Launois,*[c] Milo S. P. Shaffer *[ab] and Agnieszka Brandt-Talbot *[b]

Received 9th June 2025, Accepted 4th August 2025
DOI: 10.1039/d5fd00099h

Lignin is an attractive raw material for low-cost sustainable carbon fibres, however, the resulting mechanical properties require improvement before they can be implemented in composite applications. The mechanical properties of conventional polyacrylonitrile-derived carbon fibres depend critically on the molecular alignment induced in the polymer fibres by fibre drawing and on retention of the alignment during subsequent thermal treatments. In this study, alignment was induced in high lignin content fibres wet-spun from a low-cost ionic liquid water mixture by employing similar hot-drawing methods. 75/25 wt/wt% lignin–poly(vinyl alcohol) (lignin–PVA) fibres were continuously wet-spun from a 60/40 wt/wt% *N*,*N*-dimethylbutylammonium hydrogen sulfate, [DMBA][$HSO_4$] water mixture, using deionised water used as the coagulant. Hot-drawn fibres with high draw ratios of up to 20 were generated at 180 °C. By careful selection of the initial extrusion diameter and the subsequent draw ratio, the influence of fibre diameter and draw ratio was systematically distinguished. The draw ratio was found to dominate the mechanical properties of the ductile precursor fibres, while the fibre diameter was more significant after stabilisation. The precursor fibres that experienced the highest draw ratios had tensile strengths of 235–249 MPa (up to four times higher than the undrawn lignin–PVA fibres) and tensile modulus of 7.5–8.2 GPa, while the fibre diameter was reduced from 64–106 μm to 15–23 μm. Wide-Angle X-ray Scattering (WAXS) studies showed that hot-drawing induced orientation and crystallisation of PVA at high draw ratios. The crystallisation and orientation of PVA was lost during the slow oxidative stabilisation at 250 °C, associated with a plateau at around 110 MPa tensile strength and 4 GPa tensile modulus for the

[a]*Department of Materials, Imperial College London, South Kensington Campus, London SW7 2AZ, UK. E-mail: m.shaffer@imperial.ac.uk*
[b]*Department of Chemistry, Molecular Sciences Research Hub (MSRH), Imperial College London, 82 Wood Lane, London W12 0BZ, UK. E-mail: agi@imperial.ac.uk*
[c]*Université Paris-Saclay, CNRS, Laboratoire de Physique des Solides, Orsay, 91405, France. E-mail: pascale.launois@cnrs.fr*
† These authors contributed equally to the work.

 

stabilised lignin–PVA fibres, regardless of draw ratio. Improvements to the stabilisation aimed at retaining alignment are proposed.



# Introduction

Carbon fibres are high-value components in lightweight structural composites due to their exceptional mechanical strength and stiffness. Carbon fibre reinforced composites have applications in the aerospace and automotive industries, and for the construction of wind turbines, which aid decarbonisation.[1] The majority of commercial carbon fibres are produced from the pyrolysis of fibres wet-spun from poly(acrylonitrile) (PAN) using expensive solvents such as dimethylformamide (DMF), dimethylacetamide (DMAc) or dimethyl sulfoxide (DMSO).[2] The precursor fibres undergo oxidative thermal stabilisation to cross-link the polymers before pyrolysis (carbonisation) and graphitisation.[2,3] While PAN carbon fibres have excellent mechanical properties, widespread application is limited by the high cost of carbon fibre manufacturing. Generating the precursor fibre contributes to around 50% of the carbon fibre production cost.[4] Moreover, PAN is derived from fossil fuel feedstocks, which links the material to global warming. Alternative precursors made from renewable feedstocks are needed to obtain carbon fibres with improved sustainability and at reduced production cost, together with mechanical properties that are sufficient for target applications.[5–9] The United States Department of Energy (DoE) has determined a target of 1.72 GPa tensile strength and 172 GPa tensile modulus at a price of <$10 per kg for low-cost sustainable carbon fibres for general automotive applications, 50% below the $20 per kg for standard modulus carbon fibres (3.5 GPa tensile strength and 230 GPa tensile modulus).[4,10]

Carbon fibres can be produced from lignin, an abundant polymer present in wood biomass. Lignin is biosynthesised from cinnamic alcohols *via* radical polymerisation and has no defined repeating sequence.[11] Technical lignins are available as a low-cost by-product of chemical pulping, which is focused on isolating wood cellulose for fibre and dissolving applications.[12,13] They are typically complex mixtures of macromolecules, with structural motifs varying with the botanical source and the extraction method. Kraft pulping is one of the two industrially applied chemical pulping processes, with Kraft cellulose pulp widely used in paper, hygiene and packaging applications. The Kraft lignin is typically incinerated during the recovery of the pulping chemicals but can be isolated from the black liquor using LignoBoost precipitation.[14] Valorising lignin into value-added materials is a route towards product diversification for Kraft pulp mills, resulting in increased sales volumes and profits. Lignins have been spun into fibre-form either alone or, more often, blended with polymers.[15] Lignin precursor fibres can be produced by melt-spinning, wet-spinning or dry-spinning.[16,17] When solvents are used for fibre formation during wet-spinning, the cost of the solvents is important, and a fibre-forming additive must be used as the intermolecular interactions in lignin are too weak to maintain integrity during coagulation, indicated by low solution viscosities. Yang *et al.* developed a low-cost approach to wet-spinning high lignin content precursor fibres, with up to 90% lignin content. Partially acetylated poly(vinyl alcohol) (PVA) was employed as the fibre-forming additive, while a low-cost ionic liquid (IL) water mixture was used as the

solvent and pure water as the coagulation (non-) solvent.[18] The ionic liquid is projected to cost around $1 per kg, which is 3–5 times cheaper than PAN spinning solvents such as DMSO,[19,20] with production cost of ionosolv spun carbon fibre estimated as $9.02–$9.69 per kg.[21] The morphology of the carbonised fibres was ideal (circular and smooth surfaces), however, the proof-of-concept carbon fibres derived from Kraft softwood lignin (54–100 μm diameter) only had around 0.45 GPa tensile strength and 40 GPa tensile modulus.[18] The mechanical properties are below the best mechanical performance reported for biobased carbon fibres containing lignin, which is 2.45 GPa tensile strength[22] and 279 GPa tensile modulus,[23] between the DoE target and standard modulus carbon fibres. Publications reporting state-of-the-art mechanical performance for renewable, lignin derived carbon fibres are listed in Table S1, SI. The modest performance was expected given that the fibres were produced *via* a rotating bath method that did not permit tensioning after coagulation.

Fibre diameter is an important processing parameter that influences tensile strength, as it correlates with the defect size and density, factors which control brittle failure; commercial carbon fibres are typically only 5–10 μm in diameter.[24,25] Molecular alignment is also critical to the performance of polymer fibres; in the case of carbon fibres, the orientation of the precursor molecules plays a major role in determining the alignment of the graphitic planes after carbonisation, which in turn influences mechanical performance, especially stiffness. Applying tension during fibre processing through gel-drawing and hot-drawing steps is a key tool to increase axial alignment, in addition to maintaining the alignment during the subsequent thermal transformations that convert the polymer precursor into carbon.[26] The optimisation of these steps has been critical to the industrialisation of PAN carbon fibres, and the continued improvement in their properties. Although more rarely applied, drawing also improves the mechanical properties of lignin-derived carbon fibres; Luo *et al.* showed that stretching melt-spun organosolv lignin fibres using controlled and increasing tensioning during a prolonged stabilisation process improved the average tensile strength of the carbonised fibres from 549 MPa to 2.12 GPa and the average tensile modulus from 48 GPa to 189 GPa.[22] Vaughan *et al.* combined stretching of melt-spun fibres containing a 50/50 wt/wt% blend of organosolv lignin and a biobased thermoplastic polyurethane with the application of UV-irradiation as a cross-linking agent, generating high stiffness lignin carbon fibres with 279 GPa tensile modulus.[23]

A variety of wet/hot-drawing processes are applied commercially to thermoplastic PVA fibres to reduce the fibre diameter, improve orientation and induce crystallisation, resulting in better mechanical properties.[27–30] Some examples are also known for lignin–PVA fibres. Föllmer *et al.* showed that the tensile strength of 70/30 wt/wt% Kraft lignin–PVA fibres, wet-spun from DMSO into isopropanol, was increased from around 80 MPa to 200 MPa when hot-drawing with a draw ratio of 2.[31] Alignment of PVA has also been reported for continuously-spun lignin–PVA fibres with 5–50% lignin content, gel-spun from DMSO into methanol/acetone and hot-drawn in four stages at temperatures between 100 °C and 240 °C, generating fibres with a tensile strength of around 0.75 GPa and a modulus of around 30 GPa.[32]

This work develops the wet-spinning of lignin–PVA fibres with a lignin content of 75% from an ionic liquid water mixture into a continuous process. Hot-drawing

is then applied to induce molecular alignment and reduce the fibre diameter; both factors are expected to improve performance. Since they are coupled, a systematic series of experiments was designed to investigate which factor is more important for these high lignin content lignin–PVA fibres.



## Results and discussion

### Continuous wet-spinning of lignin–PVA fibres

Our previous work extruded lignin–PVA dope solutions (75/25 wt/wt%) into a rotating coagulation bath; the viscous drag of the coagulant (water) in the water bath provided the force to draw the fibres from the needle in a controlled fashion.[18] Here, wet-spinning of lignin–PVA fibres was performed using a continuous spinning line, generating ~4 m long single filaments which were wound onto rolls. In addition to being more relevant to scale-up, continuous spinning has several advantages, for example, longer lengths of more consistent fibres can be produced more quickly. Variation of the ratio between extrusion speed and collection speed may also reduce the fibre diameter and induce some alignment during coagulation. Additional processes, including washing, drawing, heating, and drying can be implemented in-line; however, offline exploration can help to understand the efficacy of each step before combining them.

Extrusion of the lignin–PVA fibres was indeed possible at a faster rate (2.5 mL $h^{-1}$) on the continuous line compared to batch-wise processing used by Yang *et al.* (at 0.6 mL $h^{-1}$).[18] A photo of a fibre that was collected and air-dried on the roll can be seen in the SI in Fig. S1. Extrusion through two needle spinnerets of different sizes was demonstrated, one with 159 μm inner diameter (30 G) and one with 260 μm inner diameter (25 G). For the lignin–PVA fibres extruded through the smaller diameter (30 G) needle, a maximum relative collection rate of $0.8v_e$ (0.8 times the linear extrusion velocity) was achieved. Faster collection rates resulted in fibre breakage. The 25 G fibres could be collected at faster speeds, at least up to $1.6v_e$, but the take-up rate was maintained at $0.8v_e$ for consistency in this study.

As the fibres were collected on the roll while wet, the circular cross-sections of the lignin–PVA fibres that form during coagulation were not retained after collection. During drying, solvent evaporation from the continuous fibres under tension induced anisotropic shrinkage along the fibre axis, generating normal contact forces at the fibre–roll interface (Fig. 1). The flattened shape may affect the fracture mechanics and result in the underestimation of tensile properties, however, trends should not be affected. Including a drying step in the continuous spinning will eliminate the deformation in the future. For commercial applications, carbon fibres are typically circular, but other shapes are also used, for example, so called "kidney bean" fibres, such as Toray's M55 grade.

Fibre diameters for the air-dried 30 G and 25 G as-spun fibres were 64 ± 3 μm and 106 ± 5 μm, respectively. These fibre diameters were either similar to or smaller than those obtained by Yang *et al.* (100–120 μm) using a rotating coagulation bath and 27-gauge (210 μm diameter) spinneret for the same dope composition.[18] A similar diameter for different spinnerets suggests that the dope viscosity may have varied between the spinning dopes used in this work and Yang *et al.* (lower viscosities generate smaller fibre diameters). The dope viscosity can be adjusted through the dope composition, using a range of factors such as polymer ratio, the lignin and PVA type, and also dope ageing time.[18,21] The 25 G

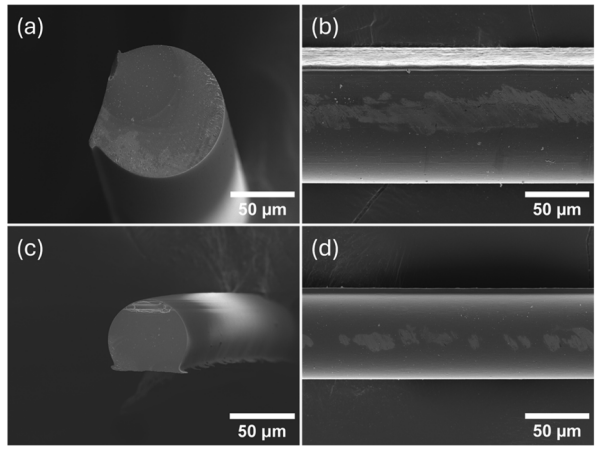


Fig. 1 SEM images of air-dried as-spun Kraft lignin–PVA fibres spun continuously from [DMBA][$HSO_4$] and water mixtures using a 25 G (260 μm) spinneret (a and b) and a 30 G (159 μm) spinneret (c and d).

and 30 G as-spun fibres had similar tensile strengths ($50 \pm 9$ MPa and $55 \pm 6$ MPa, respectively), an improvement on the wet-spun fibres produced by Yang *et al.* using a rotating spinning bath, with tensile strengths of around 37 MPa.[18] The moduli of the continuously spun fibres ($5.0 \pm 0.8$ GPa and $4.6 \pm 0.2$ GPa) were similar to the batch-spun fibres (around 4.8 GPa) reported previously. The estimated carbon yield for the continuously-spun lignin–PVA fibres (38.0%), determined by TGA under nitrogen (Fig. S2), matched the estimated carbon yield measured for the Kraft lignin fibres batch wet-spun by Yang *et al.* ($36 \pm 2.8$%).[18]

## Hot-drawing

Hot-drawing applies heat to a fibre to increase the mobility of polymers in the material and allow for reorientation of polymer molecules under mechanical tension; elongation tends to lead to improved molecular alignment. Depending on the type of polymer, different temperatures are suitable for hot-drawing. To determine a suitable hot-drawing temperature for the lignin–PVA system, the air-dried as-spun fibres were subjected to hot-drawing over a range of temperatures, using a continuous single fibre processing unit. Temperatures from between 140 and 240 °C in 20 °C increments were investigated. At 200 °C and above, the fibres were deformed due to the evolution of bubbles from within, likely a result of rapid evaporation of water present in the air-dried lignin–PVA blend (4.7 wt%, calculated from the TGA), although volatile products may also be generated by reactions in the lignin PVA fibres, as indicated by TGA measurements (Fig. S2). At temperatures below 180 °C, fibre elongation was observed but the maximum draw ratio (DR) was limited to 12 before the fibres broke. It was found that an exceptionally high DR of 20 was accessible at 180 °C without the occurrence of bubbling, hence this temperature was used for further investigation. The suitability of 180 °C as the hot-drawing temperature can be explained with DSC measurements, shown in the SI in Fig. S3, which determined a glass transition temperature for the lignin ($T_g = 169$ °C), and a melting transition for the PVA

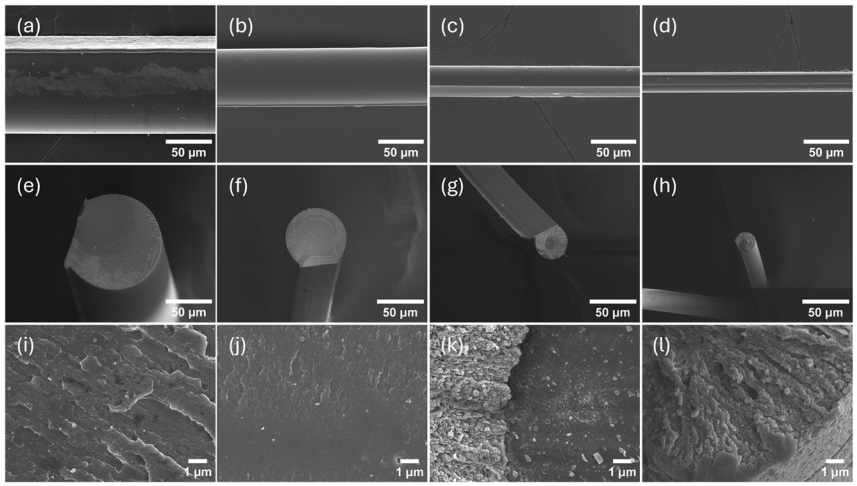


Fig. 2 SEM images of the fibre lengths of 25 G as-spun lignin–PVA fibres (a), and hot-drawn fibres at 180 °C to DR 2.5 (b), DR 8 (c), and DR 20 (d). The respective cross-sections are seen at the same magnification (e–h) and at higher magnification (i–l).

(160–200 °C, with the peak at 190 °C in pure PVA and the as-spun lignin PVA fibre). The DSC thermograms indicate that the temperature providing the highest draw ratio (180 °C) was above the $T_g$ of the lignin (~170 °C) and close to the maximum of PVA melting transition.

SEM images of as-spun and drawn fibres (Fig. 2) show that the hot-drawn fibres retained longitudinally consistent diameters, with the flattened fibre shapes preserved. The fibre diameters decreased with increasing draw ratio; fibres obtained with DR 20 had a diameter below 30 μm, a more than 3-fold reduction compared to the as-spun fibres. The drawn fibres had smooth surfaces but an increasingly rugged cross-sectional fracture surface. A similar pattern has been observed on the cross sections of hot-stretched polyethylene fibres and is attributed to the formation of fibrillar crystals.[33]

To distinguish between the effect of decreasing fibre diameter and induced polymer orientation on the properties of drawn lignin–PVA fibres, a series of drawing experiments were performed up to the maximum possible draw ratio of 20, with the draw ratios selected to achieve matching diameters for the 30 G and 25 G fibres. Fig. 3 shows the relationship between increasing draw ratio and reducing fibre diameter for the hot-drawn fibres. As expected, the fibre diameter scaled with the reciprocal square root of the draw ratio, consistent with the assumption that the fibre volume remains constant during hot-drawing; this assumption is consistent with the finding that mass loss only occurred above 200 °C in the TGA of air-dried lignin–PVA fibres (Fig. S2).

### Wide-angle X-ray scattering (WAXS) of hot-drawn fibres

X-ray scattering was employed to inspect the effect of drawing on the orientation of polymers in the lignin–PVA fibres. X-ray scattering images from the hot-drawn lignin–PVA fibres made with 25 G and 30 G spinnerets are shown in Fig. 4 and Fig. S4(a–d), respectively. The corresponding scattering diagrams, reporting the

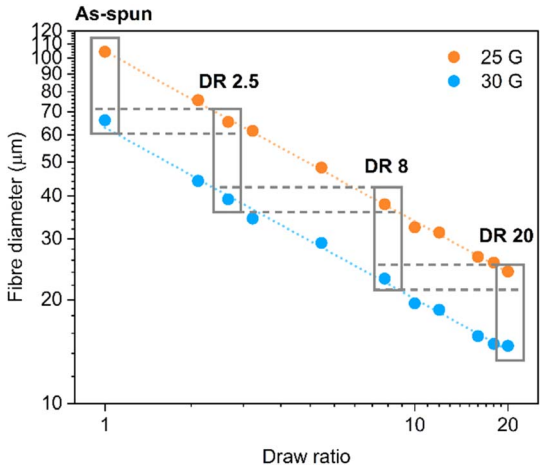


Fig. 3 Relationship between fibre diameter and draw ratio (DR) for lignin–PVA fibres extruded through 25 G (260 μm) and 30 G (159 μm) spinnerets. Vertically oriented boxes indicate fibres with the same draw ratio (but different diameter) and horizontally oriented boxes (dashed) indicate hot-drawn fibres with the same diameter (but different draw ratios). The orange and blue lines (dotted) fitted to the 25 G and 30 G data have slopes of −0.49 and −0.50, respectively.

measured intensity integrated over the azimuthal angle as a function of the wave-vector $Q$, are shown in Fig. 5(a) and Fig. S5(a). As with the mechanical properties, the flattened fibre cross section should not affect the interpretation of the WAXS results. For the as-spun fibres, a broad modulation around $Q \approx 1.4$ Å$^{-1}$ was observed and assigned to a scattering signal from both lignin (Fig. S6) and amorphous PVA, which corresponds to the interchain distance.[27] The most intense scattering signal from amorphous PVA is located around 1.4 Å$^{-1}$. The scattering diagram of the fibres hot-drawn to DR 8 indicates the presence of crystalline PVA. Its space group is $P2_1/m$, with unit cell parameters $a = 7.81$ Å, $b = 2.52$ Å, $c = 5.51$ Å and $\gamma = 91.7°$.[34] The corresponding Bragg peaks, labelled by the three Miller indices $hkl$ are shown in Fig. 4 and Fig. S4. The $10\bar{1}$ and 101 peaks of crystalline PVA appear at $Q \approx 1.39$ Å$^{-1}$, *i.e.* at around the same spacing as the intense peak of amorphous PVA, the chains being aligned along the axis $\vec{b}$ in the crystal. Crystalline PVA was also found for DR 2.5, albeit in smaller amounts, as

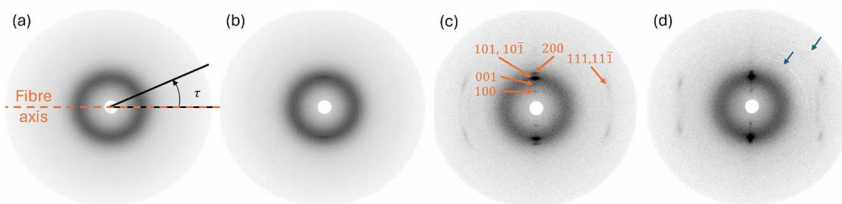


Fig. 4 WAXS patterns of 25 G as-spun lignin–PVA fibres (a), and lignin–PVA fibres hot-drawn at 180 °C to DR 2.5 (b), DR 8 (c), and DR 20 (d). The blue arrows highlight artefact rings resulting from the background subtraction. Miller indices of diffraction peaks of crystalline PVA are provided in (c).

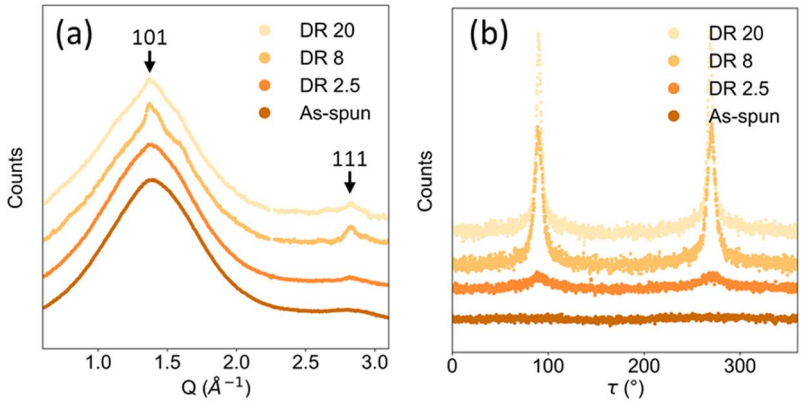


Fig. 5 (a) Scattering diagrams and (b) angular modulation of the intensity at $Q = (1.39 \pm 0.04)$ Å$^{-1}$ for the as-spun and hot-drawn 25 G fibres. Position of diffraction peaks of crystalline PVA are indicated with arrows and their Miller indices are provided Curves are translated vertically for the sake of clarity.

the peak which includes the adjacent $10\bar{1}$ and 101 peaks at $Q \approx 1.39$ Å$^{-1}$ is visible in Fig. 4(b) and Fig. S4(b).

In Fig. 4(b–d) and Fig. S4(b–d), *h0l* peaks are located perpendicularly to the fibre axis, around $\tau$ (azimuthal angle) values of 90 and 270°. It follows that the crystalline PVA domains present strong preferential orientation with respect to the fibre axis, with axis $\vec{b}$, *i.e.* the PVA chains, aligned with the fibre axis. The intensities at $Q = (1.39 \pm 0.04)$ Å$^{-1}$ as a function of $\tau$ on the detector are reported in Fig. 5(b) and Fig. S5(b). They were fitted by Lorentzian functions (Fig. S7) and their full width at half maxima (FWHM) are reported in Table 1. For the as-spun fibre, the broad ring around 1.4 Å$^{-1}$ was slightly modulated. Although both PVA and lignin contribute to the ring, the angular modulation is attributed to a preferred orientation of amorphous PVA, which is a long ($M_w$ ~100 kDa) linear polymer, rather than a preferred orientation of the Kraft lignin, which is mixture of short macromolecules with relatively wide molar weight distribution. Based on the FWHM, the polymer orientation was slightly higher for the fibres spun with the smaller diameter (30 G) spinneret, with FWHM = 89° *vs.* FWHM = 130° for the 25 G spinneret, when having experienced the same drawing conditions. This

Table 1 Full Width at Half Maximum (FWHM) for the fitted peaks of the as-spun and hot-drawn fibres spun from 25 G (260 μm) and 30 G (159 μm) spinnerets at different draw ratio (DR)

| | FWHM (°) | |
|---|---|---|
| | 25 G | 30 G |
| As-spun | 130 | 89 |
| DR 2.5 | 31 | 26 |
| DR 8 | 10 | 9 |
| DR 20 | 6 | 7 |

effect may be due to different shear stresses experienced while extruding the fibre, which was higher for fibres generated with the smaller diameter (30 G).

The FWHMs reported for the hot-drawn fibres reflect the orientation of crystalline PVA after drawing. For DR 2.5, the orientation was stronger for the 30 G fibre than for the 25 G fibre (FWHM = 26° *vs.* 31°), which may be a consequence of the increased alignment of amorphous PVA in the as-spun fibres. The orientation increased with the draw ratio, reaching FWHM = 6–7° for DR 20. The FWHMs were similar for the 25 G and 30 G fibres for draw ratios of 8 and 20, which shows that the initial conditions of fibre formation are not relevant at high draw ratios. The crystallisation and orientation in pure PVA fibres, with increasing draw ratio, is well documented in the literature.[27,30,31]

The amount of oriented polymer in as-spun fibres and in hot-drawn fibres can be considered with respect to the amount of lignin (assumed to be non-oriented due to the molecular shape) and non-oriented PVA. Precise quantification requires extensive calculations to move from reciprocal space to direct space, which are beyond the scope of this study.[35] However, the ratio of oriented PVA to non-oriented PVA and lignin can be estimated by taking the ratio of the signal areas in the reciprocal space after subtracting the signal extrapolated from smaller and larger $Q$-regions than the region of interest. It was found that these ratios where different for the larger diameter (25 G) and the smaller diameter (30 G) fibres, with a relative ratio r (25 G : 30 G) as follows: $r = 1.7$ for as-spun fibres, $r = 1.3$ for DR 2.5, $r = 1.4$ for DR 8, and $r = 1.2$ for DR 20 hot-drawn fibres. This comparison suggests that more of the oriented fraction was present in the 25 G fibres than in the 30 G fibres.

In an interesting study on lignin–PVA fibres obtained by gel spinning, Lu *et al.* argued that H-bonding between lignin and PVA allows for the alignment of lignin segments with PVA, which is correlated with the increased mechanical properties.[32] The lignin orientation factor was deduced from Raman anisotropy. It was most important for the 5–95% lignin–PVA fibres but was also present to a lesser extent for 50–50% lignin–PVA fibres. For the 75–25% lignin–PVA fibres generated in this work, using the X-ray scattering method to probe alignment, no lignin alignment was found. Indeed, no noticeable angular modulation of the broad peak in $Q$ around 1.4 $Å^{-1}$ is visible for the DR 20 fibres, as shown by the flat background in Fig. S7(d) and (h).

## Mechanical properties of hot-drawn fibres

Hot-drawing increased the tensile properties of the lignin–PVA fibres (Fig. 6(a)), with increasing draw ratio resulting in a linear increase in tensile strength. The fibre diameter had an insignificant influence on tensile strength (Fig. 6(b)).

The degree of orientation and the amount of crystalline PVA present in the hot-drawn fibres greatly influenced the mechanical properties. The highest tensile strengths were obtained at DR 20, with around a 5-fold increase over the undrawn lignin–PVA fibres; the values of 249 ± 11 MPa (25 G) and 235 ± 26 MPa (30 G) are consistent with the larger amount of oriented PVA for both DR 20 fibres observed by WAXS. The tensile moduli exhibited a similarly linear trend with draw ratio, but the fibres spun from the larger diameter (25 G) spinneret had a slightly higher modulus across the entire hot-drawing range (Fig. 6(c)), consistent with the slightly increase amount of orientated fraction observed. The improved

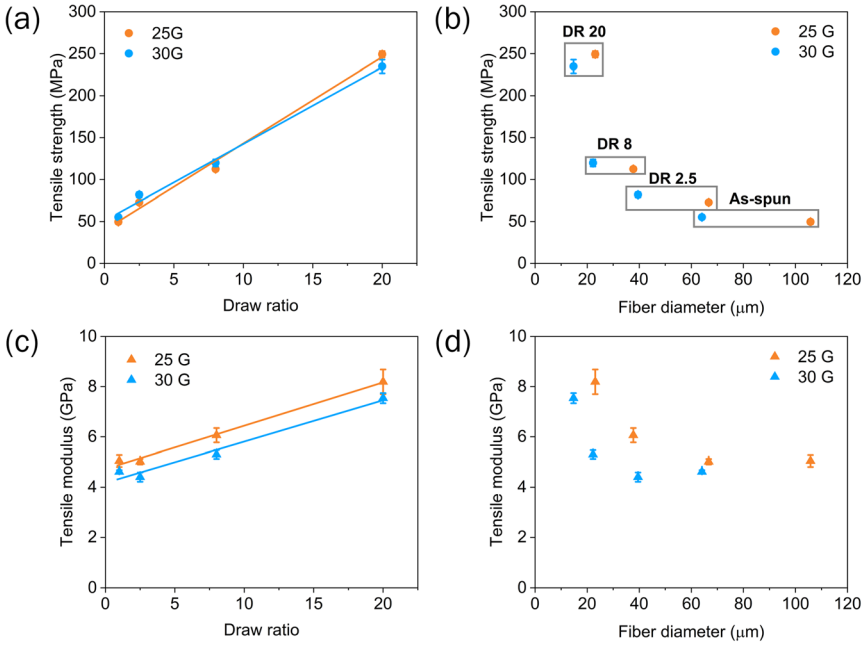


Fig. 6 Tensile strength (top) and modulus (bottom) of 25 G and 30 G lignin–PVA fibres hot-drawn to a series of draw ratios. The trend in mechanical properties is presented with respect to draw ratio, (a) and (c), and fibre diameter, (b) and (d). Horizontally oriented boxes indicate fibres subjected to the same draw ratio.

orientation and partial PVA crystallisation in DR 2.5 fibres compared to the as-spun fibres did not manifest as strongly in the tensile properties as for the larger draw ratios. In fact, the tensile modulus for DR 2.5 decreased slightly for both the 25 G and 30 G fibres. The stress–strain behaviour of the lignin–PVA fibres was more ductile after hot-drawing (Fig. S8). Overall, higher draw ratios achieve a significant improvement in mechanical properties of the lignin–PVA fibres.

### Stabilising the lignin PVA fibres

The as-spun and hot-drawn fibres were stabilised batch-wise, applying the standard protocol employed by Yang *et al.*, which uses slow temperature ramp rates of 1 °C $min^{-1}$ from 25 to 100 °C and 0.2 °C $min^{-1}$ from 100 to 250 °C in air.[18] Fixed lengths of the as-spun and hot-drawn fibres were stabilised under load to reduce the likelihood of polymer relaxation, especially in the hot-drawn fibres during the slow heating process, which would result in shrinkage in the axial direction with insufficient tension. The fibre diameters were 6–9% smaller after stabilisation under self-induced tension and the non-circular shape of the cross-sections was again preserved (Fig. 7). The stabilised fibres were characterised by tensile testing, WAXS and FT-IR spectroscopy.

### FT-IR spectroscopy of lignin–PVA fibres

FT-IR spectroscopy was used to confirm that structural changes occur in the polymers during fibre stabilisation (Fig. 8). A broad O–H stretching band (3050–

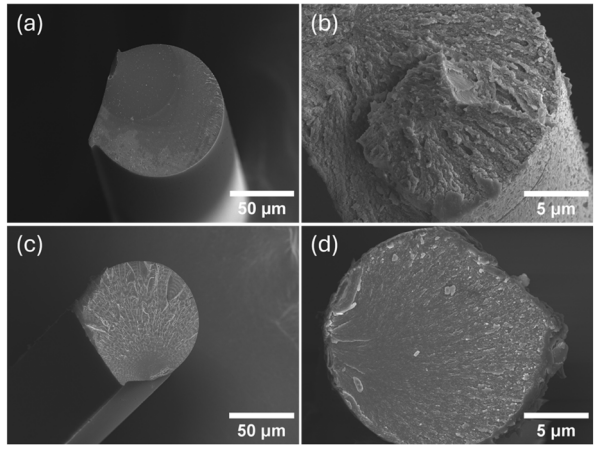


Fig. 7 SEM images of an (a) as-spun 25 G fibre, (b) 25 G fibre hot-drawn to DR 20, (c) stabilised 25 G fibre, and (d) 25 G fibre hot-drawn to DR 20 after oxidative stabilisation.

3600 $cm^{-1}$) was present in the individual polymers and the lignin PVA blend, consistent with the presence of hydroxyl group in both polymers, with the peak maximum varying for the individual polymer and the blend, indicating difference in hydrogen bonding.[36]

Stabilisation of the lignin–PVA fibres resulted in reduced intensity of O–H stretching band (3050–3600 $cm^{-1}$) and C–O stretches (1030–1260 $cm^{-1}$). The C=O stretch at 1707 $cm^{-1}$, indicative of aldehydes and carboxylic groups, remained in the stabilised fibre due to the oxidation of aliphatic O–H groups during stabilisation. More intense bands for C–H stretches and deformations (2932 $cm^{-1}$ and 1461 $cm^{-1}$), C=O stretches (1716 $cm^{-1}$), and C–C stretches (735 $cm^{-1}$) stretches (1716 $cm^{-1}$), and C–C stretches (735 $cm^{-1}$) were observed for the stabilised fibres were observed for the stabilised fibres (Fig. 8(b)), trends that have been observed for stabilised lignin fibres before.[36] A reappearance the band for C–H stretches at 2932 $cm^{-1}$ for the stabilised fibres was detected with increasing draw ratio, suggesting the formation of new aliphatic motifs.[36]

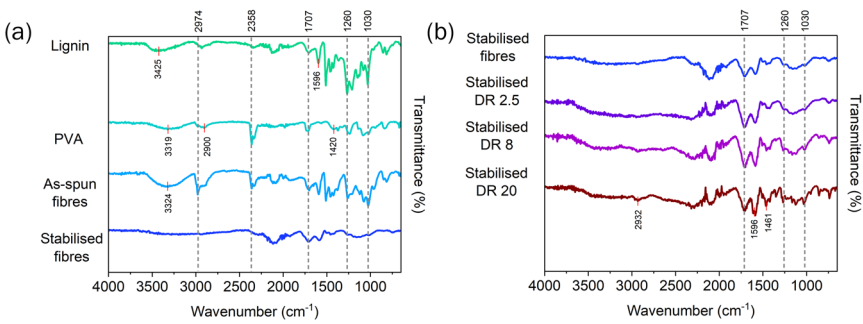


Fig. 8 FT-IR spectra of (a) Kraft softwood lignin, PVA, air-dried as-spun lignin–PVA fibres, and stabilised as-spun lignin–PVA fibres, and (b) as-spun and hot-drawn lignin–PVA fibres after oxidative stabilisation.

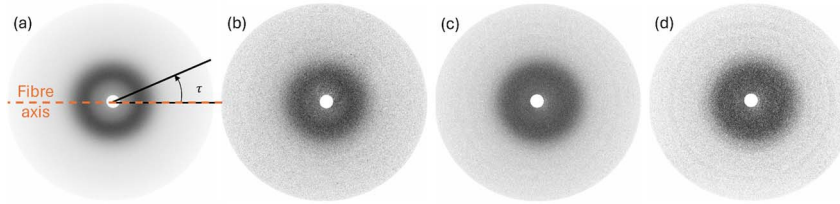


Fig. 9 WAXS patterns of 25 G lignin–PVA fibres after thermal stabilisation. As-spun and stabilised (a), and hot-drawn at 180 °C to DR 2.5 (b), DR 8 (c), and DR 20 (d) and stabilised. The smaller the fibre diameter, the weaker the signal, which leads to residual rings around 2.26 $Å^{-1}$ and 3.03 $Å^{-1}$ that persisted in the processed images even after background subtraction. The blue arrows highlight artefact rings resulting from the background subtraction.

### Wide-angle X-ray scattering (WAXS) of stabilised hot-drawn fibres

The X-ray scattering images for the thermally stabilised lignin–PVA fibres made with 25 G and 30 G spinnerets are shown in Fig. 9 and Fig. S4(e–h), respectively. Their corresponding scattering diagrams can be found in Fig. 10(a) and Fig. S5(c) and the angular dependence of the intensity at $Q = (1.39 \pm 0.04)$ $Å^{-1}$ is shown in Fig. 10(b) and Fig. S5(d). The images show that the PVA orientation and crystallisation were lost while stabilising the fibres at 250 °C, which is ascribed to the mobility of the PVA above 190 °C (Fig. S3).[28] Unexpectedly, the broad peak related to the local structure of lignin and PVA for the stabilised as-spun fibre widened and shifted to larger $Q$-values for the stabilised hot-drawn fibres (Fig. 10(a) and Fig. S5(c)). Further analysis is necessary to understand the origin of this effect in terms of the local structure in direct space.

### Mechanical properties of stabilised fibres

This study reports for the first time the tensile properties for stabilised ionic liquid spun lignin–PVA fibres. The tensile strength of the stabilised as-spun 25 G

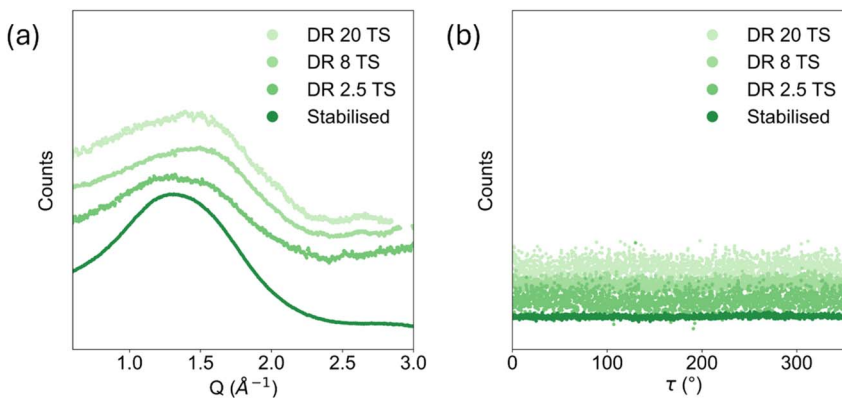


Fig. 10 (a) Scattering diagrams and (b) angular modulation of the intensity for the stabilised as-spun and hot-drawn 25 G fibres. Curves are translated vertically for the sake of clarity.

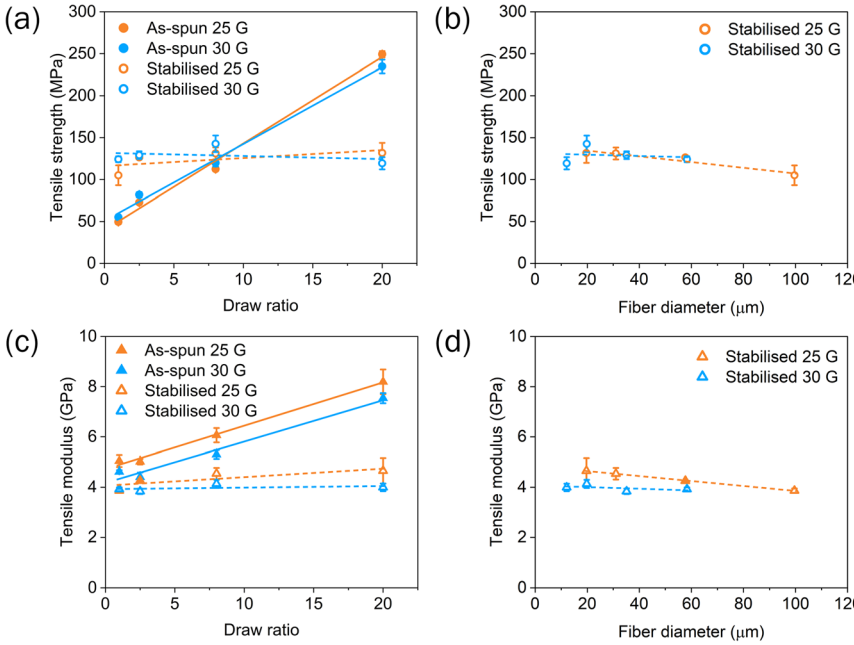


Fig. 11 Tensile strength (top) and modulus (bottom) of stabilised 25 G and 30 G lignin–PVA fibres hot-drawn to a series of draw ratios, against the properties of the unstabilised fibres. The trends in mechanical properties are presented with respect to draw ratio, (a) and (c), and fibre diameter, (b) and (d).

and 30 G fibres increased to 105 ± 26 MPa and 124 ± 11 MPa, respectively, around double that of the air-dried as-spun fibres. Increased crosslinks and healing of fibre defects during the heating ramp may account for the change in behaviour and the increased strength compared to the unstabilised as-spun fibres.

However, increasing tensile strength with increasing draw ratio was no longer observed after fibre stabilisation (Fig. 11). The loss of polymer orientation and crystallinity seen with WAXS was mirrored by the mechanical properties of the stabilised fibres, which became similar for all draw ratios. A slight decrease in tensile strength was observed with increasing diameter (Fig. 11(b)) but may not be significant. After stabilisation, the as-spun and hot-drawn fibres displayed similarly shaped stress–strain curves, with a significant yield plateau (Fig. S8). The moduli of the stabilised hot-drawn fibres were around 3.9 ± 0.2 GPa, similar to those of the as-spun fibres, again consistent with lost polymer orientation and crystallinity. There was a weak diameter effect for the modulus (Fig. 11(d)), with smaller diameter fibres having a higher tensile modulus.

In summary, using the applied stabilisation conditions, the oriented polymers relaxed before the structure was fixed, which could be responsible for the lack of trend in tensile strength with draw ratio or fibre diameter. A faster temperature ramp rate or additional drawing during stabilisation may be needed to retain the oriented structure.

# Experimental

## Materials and methods

Softwood Kraft lignin was supplied by the Research Institutes in Sweden (RISE), isolated through the LignoBoost process from black liquor derived from spruce and pine biomass. Poly(vinyl alcohol) (PVA) with an average molecular weight of 85 000–124 000 g $mol^{-1}$, 87–89% hydrolysed, was purchased from Sigma-Aldrich. The materials were used as received. The ionic liquid (IL) *N*,*N*-dimethylbutylammonium hydrogen sulfate [DMBA][$HSO_4$] was synthesised at Imperial College London using *N*,*N*-dimethylbutylamine (>99% purity) and sulfuric acid solution (66.3%) purchased from VWR.[18] The acid-to-base ratio of the ionic liquid was confirmed as 1.03 ± 0.01 using an automatic titrator (volumetric Karl Fischer titrator, Mettler Toledo V20) as discussed in previous work.[18]

## Fibre spinning

The dope solution was prepared following the method described in previous work by Yang *et al.*[18] In summary, an aqueous PVA solution was stirred for 1 h at 85 °C followed by the addition of [DMBA][$HSO_4$] and softwood Kraft lignin. This dope solution was stirred for 1 h at 60 °C and allowed to cool to room temperature. The final dope composition was 3 : 1 lignin : PVA at 16% solid loading in a [DMBA][$HSO_4$]$_{60\%}$ $H_2O_{40\%}$ solvent. The dope solution was extruded from a 2.5 mL Gastight 1000 PTFE Luer lock (TLL) syringe (Hamilton) through $\frac{1}{2}''$ needles with two different gauges (25 G and 30 G with inner diameters of 260 and 159 μm respectively) using a high-pressure syringe pump (Chemyx Fusion 6000X) at an extrusion rate of 2.5 mL $h^{-1}$. The fibres were allowed to coagulate in a deionised water bath for an average residence time of at least 45 s and collected on a Delrin acetal roll (48 mm diameter) at 0.8 times the take-up speed relative to the linear extrusion velocity. The rolls were operated by stepper motors controlled by IC drivers (TMC2130, Trinamic) and a microcontroller (Arduino Uno) constructed at Imperial College London (winding unit). The fibres were allowed to air-dry on the roll. The wet-spinning parameters are detailed in the SI Table S2.

## Hot-drawing

The air-dried fibres were hot-drawn through a 30 cm ceramic-insulated heating zone on the conditioning unit of a microfiber line (Xplore), adapted with two Delrin acetal rolls and their stepper motors as feed-in and take-up rolls. The fibres were hot-drawn at a feed-in rate of 15 cm $min^{-1}$ to a series of draw ratios (DR 2.5, 8, and 20), where DR is a multiplier of the feed-in rate for the take-up rate (Table 2).

Table 2 Parameters for hot-drawing lignin–PVA fibres through a 30 cm heating zone

| Draw ratio | Feed in rate, cm $min^{-1}$ | Take-up rate, cm $min^{-1}$ |
|---|---|---|
| 2.5 | 15.1 | 37.7 |
| 8 | 15.1 | 120.6 |
| 20 | 15.1 | 301.6 |

### Oxidative stabilisation

The as-spun and hot-drawn fibres were fixed onto graphite frames with a gauge length of 19 cm using Glassbond Aluseal Adhesive Cement No. 2 ceramic paste and oxidatively stabilised in a Memmert UNP-200 oven following the temperature program of 1 °C $min^{-1}$ from 25 °C to 100 °C, 0.2 °C $min^{-1}$ from 100 °C to 250 °C, holding at 250 °C for 1 hour before ambient cooling to room temperature.

### Scanning electron microscopy (SEM)

The fibres were fractured and secured on aluminium stubs with carbon tape and coated with 10 nm of chromium. The fibre lengths and cross-sections were observed using a Zeiss Gemini Sigma 300 scanning electron microscope using the InLens detector with an accelerating voltage of 5 kV and an aperture of 30 μm at a working distance of 6 mm.

### Wide-angle X-ray scattering (WAXS)

Wide angle X-ray Scattering (WAXS) measurements were performed on a rotating anode X-ray generator (MicroMax 007, Rigaku Corp., Japan; 40 kV–16 mA) of the MORPHEUS platform at Laboratoire de Physique des Solides. The X-ray beam was monochromatised and collimated by a multilayer optics (FOX3D 14–39, Xenocs, France) at the copper Kα radiation ($\lambda$ = 1.5418 Å) with a beam size around 1 $mm^2$.

Experiments on fibres were performed with the sample placed in a vacuum chamber, to minimise contamination due to air scattering. 2D-WAXS diagrams were collected on a MAR345 detector (marXperts GmBH, Germany) with a 150 μm pixel size, placed behind the vacuum chamber outlet window, at a distance of 148 mm from the sample. The exposure time for each measurement was 2 hours, repeated multiple times for the small diameter fibres. Additionally, several background images were acquired without a sample for the same duration. The final images were added and subtracted by the same number of background images.

The experiment on lignin powder was performed under air, with the powder placed in a borosilicate capillary with a diameter of 0.9 mm. The sample-to-detector distance was 200 mm. A background image taken with an empty capillary was also subtracted.

To plot the scattering diagrams, the final images were integrated over the azimuthal angle on the detector, which provided the intensity as a function of the scattering wave-vector $Q$. Furthermore, the intensities on the scattering diagrams were corrected of the polarisation of X-rays and the geometrical factor for the planar detector. Angular intensity profiles were also plotted, showing the intensity changes integrated over a specific narrow wave-vector range around the wave-vector value of interest, plotted against the azimuthal angle on the detector.

### Mechanical testing

Single filaments of the as-spun, hot-drawn, and stabilised lignin–PVA fibres were mounted on card templates for tensile testing with a gauge region of 15 mm. A minimum of 10 samples per set of fibres were tested, and 15 random points along each fibre were measured for an average diameter for each fibre sample using

ImageJ applied to images taken on a Leica DM2500 optical microscope with a Basler Ace acA1920 camera. The ends were fixed using Araldite Rapid epoxy and left to cure at room temperature for 10 days before being tested. A minimum of 10 tests were conducted on each fibre, and the fibres were mechanically tested using a Linkam Scientific MFS fitted with a 20 N load cell at 1 mm $min^{-1}$ until failure at ambient temperature. The measurements were performed, and the data was processed, following ISO 11566:1996.

### Differential scanning calorimetry (DSC)

Differential scanning calorimetry (DSC) was performed to determine the melting transitions of lignin, PVA, and as-spun lignin–PVA fibres for hot-drawing. Each sample ranging from 3–7 mg was heated from 25 to 250 °C at a rate of 10 °C $min^{-1}$, cooled to 25 °C and heated again to 250 °C at the same rate under a nitrogen atmosphere (20 mL $min^{-1}$) using a TA Q2000 DSC (TA Instruments).

### Thermogravimetric analysis (TGA)

Thermogravimetric analysis (TGA) was performed using a Pyris 1 TGA (PerkinElmer) to determine the mass loss events for lignin, PVA, and as-spun lignin–PVA fibres. The sample was placed on a pre-tared high temperature platinum TGA pan, and the sample was heated from 25 to 900 °C at 10 °C $min^{-1}$ under a nitrogen atmosphere (20 mL $min^{-1}$), with an isothermal step at 100 °C for 30 minutes. The mass loss curves were plotted for the temperature range of 100–900 °C.

### FTIR-ATR spectroscopy

Attenuated total reflectance Fourier-transform infrared spectroscopy (FTIR-ATR) spectra were recorded using a Cary 630 FTIR Spectrometer (Agilent). For each measurement, 16 scans were recorded over the spectral range 4000–650 $cm^{-1}$ at a resolution of 2 $cm^{-1}$. The spectra were baselined using the peak analyser function and smoothed using the Savitzky-Golay method with the software, OriginPro 2024.

## Conclusions

Lignin–PVA fibres with a high lignin content (75%) were successfully wet-spun using a low-cost ionic liquid water mixture, using a continuous laboratory scale spinning line, developing a previous batch method. The continuous arrangement is well suited to further development to include more extensive in-line washing, gel-drawing, hot-drawing, and drying processes, compatible with conventional industrial scale-up. The possibility of applying drawing was investigated by applying offline hot drawing. Exceptionally high draw ratios, up to 20, were successfully applied, reducing the fibre diameters from 64–106 μm to 15–23 μm, which is a promising range for the diameter scales used for commercial carbon fibre production.

The hot-drawing enhanced the orientation and crystallisation of the PVA phase, which was accompanied by increases in tensile strength. The tensile strength increases were predominantly related to draw ratio, with the highly drawn fibres (DR 20) achieving five times the tensile strength of the as-spun fibres. However, the slow heating rate and possibly the long hold time during the applied

oxidative stabilisation resulted in the loss of polymer orientation, and the tensile properties of stabilised fibres were similar and independent of draw ratio. Stabilisation of softwood Kraft lignin can be performed at faster heating rates with a lower holding time,[37] therefore stabilising the hot-drawn fibres at a faster heating rate could be beneficial to lock in the oriented PVA crystallite structure. Additionally, applying stretching at temperatures closer to those needed for stabilisation while avoiding water evolution through more rigorous drying, could contribute to retaining an oriented microstructure during stabilisation.[25] If the molecular orientation in the lignin PVA can be retained through stabilisation and onwards to carbonisation, the mechanical properties of the resulting sustainable low-cost carbon fibres should be improved.

## Author contributions

ET and JPFN contributed to this study with methodology, investigation, formal analysis of the experimental lignin–PVA fibre work, visualisation, and writing the original draft. LD contributed to this study with investigation and formal analysis of WAXS experiments, visualisation, and writing of the original draft. SR contributed with methodology by designing and installing the vacuum diffusion chamber for the WAXS studies. PL, MS and ABT contributed to this study with the conceptualisation, funding acquisition, project administration, supervision and writing (review and editing).

## Conflicts of interest

There are no conflicts to declare.

## Data availability

Data supporting this article have been included as part of the supplementary information (SI) file, which contains additional details relating to wet-spinning parameters, TGA and DSC curves, WAXS diagrams, and stress–strain curves. See DOI: **https://doi.org/10.1039/d5fd00099h**. Furthermore, the repository 'Hot-drawing lignin–PVA fibres' at **https://doi.org.10.6084/m9.figshare.30219370** contains data such as unprocessed SEM and WAXS images and electronic data relating DSC, FT-IR spectroscopy and tensile testing.

## Acknowledgements

The authors thank Dr Charles M D Shaw for assistance with DSC measurements. The work was funded by the EPSRC and SFI Centre for Doctoral Training in Advanced Characterisation of Materials (EP/S023259/1), the Royce Industrial Collaboration Programme (reference EHZ2494092, ICP311) and the UKRI Impact Acceleration Account (EP/X52556X/1, PSO395). Enny Tran and Lucie Diéval acknowledge the funding of the joint CNRS-Imperial College PhD project 'Spinning sustainable carbon fibres for the energy transition'.

## Notes and references

1 J. Zhang, G. Lin, U. Vaidya and H. Wang, *Composites, Part B*, 2023, **250**, 110463.
2 E. Frank, L. M. Steudle, D. Ingildeev, J. M. Spörl and M. R. Buchmeiser, *Angew. Chem., Int. Ed.*, 2014, **53**, 5262–5298.
3 P. Gutmann, J. Moosburger-Will, S. Kurt, Y. Xu and S. Horn, *Polym. Degrad. Stab.*, 2019, **163**, 174–184.
4 T. Peijs, R. Kirschbaum and P. J. Lemstra, *Adv. Ind. Eng. Polym. Res.*, 2022, **5**, 90–106.
5 D. Choi, H.-S. Kil and S. Lee, *Carbon*, 2019, **142**, 610–649.
6 L. Yan, H. Liu, Y. Yang, L. Dai and C. Si, *Carbon Energy*, 2025, **7**, e662.
7 S.-C. Sun, Y. Xu, J.-L. Wen, T.-Q. Yuan and R.-C. Sun, *Green Chem.*, 2022, **24**, 5709–5738.
8 A. Bengtsson, J. Bengtsson, C. Olsson, M. Sedin, K. Jedvert, H. Theliander and E. Sjöholm, *Holzforschung*, 2018, **72**, 1007–1016.
9 M. P. Vocht, A. Ota, E. Frank, F. Hermanutz and M. R. Buchmeiser, *Ind. Eng. Chem. Res.*, 2022, **61**, 5191–5201.
10 Toray Composite Materials America Inc., *T300 Standard Modulus Carbon Fiber Datasheet*, 2025.
11 J. Ralph, C. Lapierre and W. Boerjan, *Curr. Opin. Biotechnol.*, 2019, **56**, 240–249.
12 S. Rawat, A. Kumar and T. Bhaskar, *Curr. Opin. Green Sustainable Chem.*, 2022, **34**, 100582.
13 A. Brandt-Talbot, F. J. V. Gschwend, P. S. Fennell, T. M. Lammens, B. Tan, J. Weale and J. P. Hallett, *Green Chem.*, 2017, **19**, 3078–3102.
14 P. Tomani, *Cellul. Chem. Technol.*, 2010, **44**, 53–58.
15 D. A. Baker and T. G. Rials, *J. Appl. Polym. Sci.*, 2013, **130**, 713–728.
16 M. Zhang and A. A. Ogale, *Carbon*, 2014, **69**, 626–629.
17 J. Jin, J. Ding, A. Klett, M. C. Thies and A. A. Ogale, *ACS Sustain. Chem. Eng.*, 2018, **6**, 14135–14142.
18 S. M. Yang, M. S. P. Shaffer and A. Brandt-Talbot, *ACS Sustain. Chem. Eng.*, 2023, **11**, 8800–8811.
19 M. Morales, PhD thesis, ETH Zurich, 2016, DOI: **10.3929/ethz-a-010797794**.
20 L. Chen, M. Sharifzadeh, N. Mac Dowell, T. Welton, N. Shah and J. P. Hallett, *Green Chem.*, 2014, **16**, 3098–3106.
21 S. M. Yang, R. I. Muazu, E. Tran, C. B. Talbot, N. Shah, M. S. P. Shaffer and A. Brandt-Talbot, *RSC Sustainability*, 2025, **3**, 3972–3986, DOI: **10.1039/D5SU00218D**.
22 Y. Luo, M. E. A. Razzaq, W. Qu, A. A. B. A. Mohammed, A. Aui, H. Zobeiri, M. M. Wright, X. Wang and X. Bai, *Green Chem.*, 2024, **26**, 3281–3300.
23 M. Vaughan, A. Beaucamp and M. N. Collins, *Composites, Part B*, 2025, **292**, 112024.
24 R. Moreton and W. Watt, *Nature*, 1974, **247**, 360–361.
25 D. J. Johnson, *J. Phys. D: Appl. Phys.*, 1987, **20**, 286–291.
26 H. Lee, L.-W. Lee, S.-W. Lee, H.-I. Joh, S.-M. Jo and S. Lee, *e-Polym.*, 2014, **14**, 217–224.
27 Q. Wu, N. Chen, L. Li and Q. Wang, *J. Appl. Polym. Sci.*, 2012, **124**, 421–428.
28 Q. Wu, N. Chen and Q. Wang, *J. Polym. Res.*, 2010, **17**, 903–909.
29 C.-A. Link, K.-S. Hwang and C.-H. Lin, *J. Polym. Res.*, 1994, **1**, 215–219.

30 K.-S. Hwang, C.-A. Lin and C.-H. Lin, *J. Appl. Polym. Sci.*, 1994, **52**, 1181–1189.
31 M. Föllmer, S. Jestin, W. Neri, V. S. Vo, A. Derré, C. Mercader and P. Poulin, *Adv. Sustainable Syst.*, 2019, **3**, 1900082.
32 C. Lu, C. Blackwell, Q. Ren and E. Ford, *ACS Sustain. Chem. Eng.*, 2017, **5**, 2949–2959.
33 Z. Wang, M. An, H. Xu, Y. Lv, F. Tian and Q. Gu, *Polymer*, 2017, **120**, 244–254.
34 C. W. Bunn, *Nature*, 1948, **161**, 929–930.
35 V. Pichot, S. Badaire, P. A. Albouy, C. Zakri, P. Poulin and P. Launois, *Phys. Rev. B:Condens. Matter Mater. Phys.*, 2006, **74**, 245416.
36 J. L. Braun, K. M. Holtman and J. F. Kadla, *Carbon*, 2005, **43**, 385–394.
37 I. Norberg, Y. Nordström, R. Drougge, G. Gellerstedt and E. Sjöholm, *J. Appl. Polym. Sci.*, 2013, **128**, 3824–3830.